Reassessment of the Binary Mn–Rh Phase Diagram and Experimental Investigations of the Ternary Bi–Mn–Rh System

Peter Kainzbauer[1] · Martin C. J. Marker[1] · Klaus W. Richter[1]

Abstract The binary manganese–rhodium (Mn–Rh) phase diagram was reinvestigated from 5 to 90 at.% Rh with focus on determining the transition temperature between the ordered γ'-Mn$_3$Rh and the γ-Mn phase as well as the transition temperature between of the tetragonal and cubic MnRh phase and phase boundaries, applying XRD, DTA and SEM including EDX. A reassessment of the Mn–Rh phase diagram based on obtained and literature data is given. Furthermore, the phase equilibria of the ternary bismuth–manganese–rhodium (Bi–Mn–Rh) system were experimentally investigated, focusing on the possible existence of new ferromagnetic phases. Isothermal sections at 330 °C and 600 °C were studied applying powder XRD and EDX. The corresponding phase diagram was established based on these results. No additional ferromagnetic phase was found in the ternary system.

Keywords Phase diagram · Mn–Rh system · Mn–Bi–Rh system · ternary alloy system

1 Introduction

In the near future an increasing demand for rare earth elements (REEs), particularly for the production of efficient permanent magnets, will be a major factor for both cost and availability of these elements. Thus, an intensive search for REEs free ferromagnetic materials has taken place since several decades. A comprehensive review on potential compounds was published by Kramer et al.[1]

The low temperature modification α-BiMn is, among other Mn-based compounds, a possible candidate for REE free ferromagnetic materials. The α-BiMn phase crystallizes in the hexagonal NiAs type structure (space group $P6_3/mmc$) and is stable up to 355 ± 2 °C, where it decomposes in a peritectic reaction into a Bi-rich liquid and the high-temperature non-ferromagnetic β-BiMn modification, Marker et al.[2] Despite several decades of intensive research[2–6] it has not been achieved to synthesize the intermetallic α-BiMn phase as a single-phase bulk material without impurities. A possible approach to circumvent the syntheses difficulties comprises the addition of a third component to stabilize the ferromagnetic phase. Such a component can be a transition metal e.g. Ni and Rh or a metalloid like Sb that forms intermetallic phases with Bi or Mn respectively, which are iso-typic to α-BiMn.[7–9]

Lee et al.[10] reported that Rh stabilizes the non-ferromagnetic high-temperature β-BiMn modification to lower temperatures (between 324 and 329 °C) while Taufour et al.[11] described a ferromagnetic compound of BiMn$_{1.05}$Rh$_{0.02}$ (space group $Fdd2$; Curie temperature: 143 °C). Suits[12] discovered ferromagnetism in Bi substituted cubic β-MnRh (composition Bi$_x$Mn$_{1-x}$Rh; Curie temperature: − 88 °C) and ternary phases were found by Street et al.[13] (Bi$_4$Mn$_5$Rh$_2$, ferromagnetic) and Kainzbauer et al.[14] (Bi$_{18}$Mn$_5$Rh$_6$, Bi$_3$MnRh non ferromagnetic).

Based on these observations, a systematic study of the entire ternary Bi–Mn–Rh system at 330 °C (where binary α-BiMn is stable) and 600 °C (where an equilibration of Bi-poor composition appeared to be possible) was considered to be of interest, which might reveal the existence

✉ Peter Kainzbauer
peter.kainzbauer@univie.ac.at

1   Department of Inorganic Chemistry – Functional Materials, Faculty of Chemistry, University of Vienna, Althanstrasse 14, 1090 Vienna, Austria

of additional intermetallic phases, comprising ferromagnetic properties.

During this study, it turned out that the binary Mn-Rh phase diagram is still not fully understood. The most recent assessment[15] is mainly based on data obtained by Raub and Mahler[16] from 1955. In particular, nothing is known about the phase equilibria and transformation temperatures of the two intermetallic phases γ'-Mn$_3$Rh and β-MnRh. This fact triggered investigations on the γ'-Mn$_3$Rh phase with focus on the determination of the transition temperature between the γ'-Mn$_3$Rh and γ-Mn phase. A reassessment of the binary phase diagram consisting of obtained and available literature data is given here.

2 Literature Overview

2.1 The Binary Systems

Experimental phase diagram information on the two Bi containing binary boundary systems was taken from own published work and other literature. For the Bi-Rh system, the revised phase diagram by Kainzbauer et al.[17] was used as a basis, whereas the phase diagram compilation of Massalski et al.[15] provided information on the Bi–Mn system. The Mn-Rh phase diagram information is based on the reassessment of the phase diagram given in the current study.

The Bi–Mn phase diagram is accepted as shown in Reference [15] however the crystal structure of the high-temperature β-BiMn phase is disputed. The phase itself decomposes peritectically at 446 °C into liquid and α-Mn, it is formed in the reaction β-BiMn = α-BiMn + α-Mn at 340 °C. The crystal structure was, based on high-temperature neutron diffraction, originally described as hexagonal and isotypic to Ni$_2$In by Roberts[18] and Andresen et al.[19] Later Chen[20] reported a large orthorhombic supercell structure for a from 430 °C rapidly quenched BiMn$_{1.08}$ composition. This observation is consistent with the result of Andresen et al.,[19] who also investigated a rapidly quenched sample. In another study,[21] the latter authors proposed the orthorhombic structure with the space group $P222_1$ and lattice parameters of $a = 4.332(2)$ Å, $b = 7.505(4)$ Å, $c = 5.959(7)$ Å, which was later changed to the space group $Pmma$.[22]

Information on the Mn-Rh system was also obtained from the compilation in, Reference [15] which is mainly based on evaluations by Raub and Mahler[16] and Hellawell.[23] However, the available data were supplemented with a number of more recent data.

Raub and Mahler[16] established the complete phase diagram by data generated from light microscopic and powder x-ray diffraction (XRD) analyses but without any thermoanalytic methods. The samples they used were annealed between 550 and 1300 °C. The phase boundaries are extrapolated from determination of lattice parameter as a function of the concentrations. Hence, the phase boundaries are only estimated, in particular the boundaries of the two-phase fields β-MnRh + Rh solid solution and β-MnRh + γ-Mn solid solution, respectively are rendered to be to of considerable inaccuracy. Also, the solid phase transition temperature between the ordered γ'-Mn$_3$Rh and the γ-Mn solid solution are not clear yet. Later studies dealing with the phase transformation of MnRh from the cubic CsCl to the ordered tetragonal CuAu(I) type structure reported in Reference [24–26] and the work by Selte et al.,[27] are not considered in compilation.[15]

Apart from a large number of computational studies on the magnetic properties of the β-MnRh and the γ'-Mn$_3$Rh phases (e.g. in Lit.[28,29]) and experimental investigations by Yamauchi et al.,[30–33] there are no recent data on the Mn-Rh binary system.

Massalski et al.[15] shows a temperature independent phase field of the cubic MnRh phase between 35 and 55 at.% Rh. Selte et al.[27] determined the phase boundary of cubic MnRh between 42 and 50 at.% Rh, by cell dimension investigations. The authors did not specify their annealing temperature, they only mentioned that the samples were quenched to room temperature from temperatures between 500 and 950 °C. This is in good agreement with Kouvel et al.,[25] who reported the exclusive existence of the cubic MnRh phase in a quenched sample, containing 48.8 at.% Rh and annealed at 1000 °C, 800 °C and 600 °C only respectively. In contrast to the study of Raub and Mahler,[16] where the authors explicitly pointed out that no tetragonal distorted phase, known from other Mn—PGE (platinum group elements) systems, could be found, Kouvel et al.[25] observed a martensitic transformation of MnRh from the cubic to the tetragonal phase by cooling the sample to about − 193 °C. This transformation was confirmed by Nakayama and Asanuma,[26] who showed by DTA measurements, that the transition point between cubic and the tetragonal phase has a large temperature hysteresis and is decreasing with increasing Rh content. Selte et al.[27] found the tetragonal phase stable between 36 ± 0.5 to 50 ± 1 at.% Rh at liquid N$_2$ and He temperatures. Depending on the sample preparation, the tetragonal phase shows different homogeneity ranges. The existence of a pure tetragonal phase was only observed in samples which were slowly cooled down to room temperature.

There are also several discrepancies in the published works concerning the two-phase field of the β-MnRh and γ'-Mn$_3$Rh or γ-Mn phases, respectively. In Reference [15] a transition temperature from the γ'-Mn$_3$Rh to the γ-Mn phase at 520 °C is described in the range of 32 to 35 at.% Rh. Again, these values are inherited from Raub and

284

J. Phase Equilib. Diffus. (2020) 41:282–298

Mahler[16] where the origin of the transition temperature is not clear and the borders to the single-phase fields are only estimated. Selte et al.[27] interpolated the range of two phase field, from investigations of the unit cell dimensions, between 28 and 31 at.% Rh at room temperature. At liquid N_2 and He temperatures, the authors found the two phase field between 32 and 36 at.% Rh.

Yamauchi et al.[32] investigated the lattice parameters between 15 and 30 at.% Rh in ordered (annealed at 600 °C) as well as disordered (no annealing temperature given) samples, whereby they noted that there is no evident difference of lattice parameters between the ordered and disordered alloys.

In their plots Yamauchi et al. showed, for a sample containing 25 at.% Rh at 600 °C, a lattice parameter c of 3.812 Å[32] and 3.815 Å[33] respectively. Both are in good agreement with the results of Krén et al.[34] who report a c value of 3.813 Å for 700 °C. A graphical interpolation of the temperature dependence of the lattice parameters for a stoichiometric γ'-Mn_3Rh phase, measured between room temperature and 826 °C,[30] exhibit a lattice parameter $c = 3.836$ Å at 600 °C.

The Néel temperature of a stoichiometric γ'-Mn_3Rh sample was identified by Neutron diffraction at 580 ± 10 °C,[34] whereas 560 °C and 580 °C were observed for ordered $Mn_{77}Rh_{23}$ and $Mn_{75}Rh_{25}$ alloys in DSC measurements.[30] In further studies Yamauchie et al. denoted the Néel temperature for an ordered $Mn_{80}Rh_{20}$ alloy at 529 °C,[32] determined by magnetic susceptibility measurements, and 568 °C for an ordered $Mn_{75}Rh_{25}$ alloy.[33]

A list of crystallographic data for relevant compounds is given in Table 1.

2.2 Ternary Bi–Mn-Rh Phase

Except of the ternary phases mentioned in the introduction, no information is available on the ternary Bi–Mn–Rh system. Neither a calculated nor an experimental phase diagram is published.

3 Experimental

3.1 Sample Preparation

Binary Mn-Rh and ternary Bi–Mn–Rh bulk samples were prepared from pure elements Bi (99.999%, ASARCO, New Jersey, USA), Mn (99.95%, Alfa Aesar, Johnson Matthey Chemicals, Karlsruhe, Germany) and Rh powder (99.95% ÖGUSSA, Austria). Bi and Mn metals, except for Rh powder, were manually pulverized and sieved (grain size < 0.09 mm). Proper amounts of the powders were mixed and pressed to pellets in a 5 mm pressing cylinder under a load of 20-25 kN. To prevent the oxidation of Mn, all samples were kept and manipulated in a glove box (Labmaster SP MBraun, moisture and oxygen level below 0.1 ppm) under Ar atmosphere.

All ternary samples were annealed at 330 °C and some those annealed at 600 °C were prepared as sintered pellets. The pellets were sealed into evacuated silica glass tubes (7.0-5.0×10^{-3} mbar) comprised a small alumina plate at the bottom, and covered with a silica glass cover to reduce the gas volume (annealing time of 4 months). After the annealing process the samples were quenched in cold water. Alternatively, the samples annealed at 600 °C were prepared by placing the powder pellets into alumina crucibles which were sealed into evacuated silica glass tubes (7.0-5.0×10^{-3} mbar) and heated up to 1100 °C for 5 min, then cooled down to 600 °C within 30 min. All heating and annealing processes were carried out in muffle furnaces (Nabertherm, Germany) with a temperature accuracy of approximately ± 10 °C depending on the sample location.

Binary Mn-Rh samples were alloyed in an electric arc furnace (Bühler MAM) on a water-cooled copper plate under Ar, using Zr as getter material. Except for two samples containing 34 and 40 at.% Rh, all annealing processes of binary samples were carried with same procedure as for ternary alloys. The latter samples were instead slowly cooled to room temperature.

The manual pulverization of quenched binary samples containing the γ'-Mn_3Rh or the cubic β-MnRh phase was not possible due to their extreme toughness, necessitating a file off followed by stress annealing. Before performing XRD analysis, the filed powders were annealed for 24 h to remove the internal stress. Samples containing the tetragonal β-MnRh phase were manually pulverized in liquid N_2 instead of filing.

Details of the annealing parameters are listed in Table 2.

3.2 Characterization

Metallographic investigations on polished samples were performed with a scanning electron microscope (SEM) (Zeiss Supra 55 VP) coupled with an energy-dispersive X-ray spectroscopy (EDX). Backscattered electrons were used to visualize the surface at 20 kV acceleration voltage. The energy and intensity calibration of the EDX detector was accomplished with pure elements of Co, Mn and a $Bi_{50}Rh_{50}$ standard. To minimize statistical errors, the average phase composition was obtained from at least eight spots or area scans.

Thermal analyses were performed using a DSC 404F1 Pegasus (Netzsch, Selb, Germany), applying evacuated silica glass crucibles ($\sim 10^{-3}$ mbar) as sample containers.

J. Phase Equilib. Diffus. (2020) 41:282–298

285

Table 1 Crystal structure data of binary and ternary phases relevant for the present study

Phase	Space group	Structure type	Lattice parameters (Å)			deg (°)			V (Å³)	Ref.
			a	b	c	α	β	γ		
Bi	$R\bar{3}mH$	hR_2	4.546 (2)	4.546 (2)	11.859 (1)	…	…	…	212.27	[36]
α-Mn	$I\bar{4}_3m$	α-Mn	8.911	…	…	…	…	…	707.59	[37]
Rh	$Fm\bar{3}m$	Cu	3.8030	…	…	…	…	…	55.02	[38]
α-BiMn	$P6_3/mmc$	NiAs	4.285 (2)	4.285 (2)	6.113 (2)	…	…	…	97.2	[20]
β-BiMn	$P222_1$	–	4.334 (2)	7.505 (4)	5.959 (7)	…	…	…	193.82	[21]
BiRh	$P6_3/mmc$	NiAs	4.092 (2)	4.092 (2)	5.667 (5)	…	…	…	82.17	[17]
Bi$_4$Rh	$Ia\bar{3}d$	Bi$_4$Rh	14.930 (5)	…	…	…	…	…	3327.9	[17]
α-Bi$_2$Rh	$P2_1/c$	CoSb$_2$	6.920 (2)	6.794 (1)	6.962 (2)	…	117.73 (2)	…	289.76	[17]
β-Bi$_2$Rh	$P\bar{1}$	–	6.738 (3)	7.024 (7)	7.060 (8)	104.81 (7)	100.70 (4)	105.77 (4)	298.7	[17]
MnRh (cubic)	$Pm\bar{3}m$	CsCl	3.044	…	…	…	…	…	28.20	[25]
MnRh (tetragonal)	$P4/mmm$	CuAu	2.78	2.78	3.56	…	…	…	27.51	[25]
γ'-Mn$_3$Rh	$Pm\bar{3}m$	AuCu$_3$	3.813	…	…	…	…	…	55.43	[34]
Bi$_{18}$Mn$_5$Rh$_6$	$P4_2/mmm$	–	18.526 (3)	…	4.1722 (1)	…	…	…	1432.0 (6)	[14]
Bi$_3$MnRh	$Cmmm$	–	8.885 (3)	13.696 (6)	4.131 (1)	…	…	…	502.7 (3)	[14]
BiMn$_{1.05}$Rh$_{0.02}$	$Fdd2$	–	8.683 (3)	47.704 (8)	15.021 (3)	…	…	…	6222 (3)	[11]
BiMn$_{1-x}$Rh$_x$	$Pmma$	–	5.959 (7)	4.334 (2)	7.505 (4)	…	…	…	193.82	p.w.
Bi$_4$Mn$_5$Rh$_2$	$Fm\bar{3}m$	–	12.31	…	…	…	…	…	1865.41	[13]
Bi$_{0.2}$Mn$_{0.8}$Rh (β-MnRh(Bi))	$Pm\bar{3}m$	CsCl	3.110	…	…	…	…	…	30.08	[12]

p.w.: starting parameter for XRD refinement with Mn/Rh = 0.98/0.02 mixed occupancy of the Wyckoff position 2(d), according to Ref. [11] and [21] (please refer to text)

In order to prevent a reaction between sample and silica glass, the crucibles were protected by a carbon layer on the inside. The temperature program included two heating cycles with a heating rate of 5 K/min up to 950 °C and an equilibration step at the initial sample annealing temperature of 30 min.

Temperature measurements were performed with type S (Pt/PtRh) thermocouples calibrated at the melting points of Ag, Au, Bi and Sn. Invariant effects were evaluated from the extrapolated peak onset, both on heating and cooling. Second order transitions were evaluated from the peak maximum on heating and from the peak onset on cooling. Generally, the effects evaluated in the first heating run were deemed most reliable.

Phase identification was performed at ambient conditions by powder XRD on a Bruker D8 Advance Diffractometer in Bragg–Brentano pseudo-focusing geometry (reflection setting), using Cu-Kα radiation and a LynxEye® one-dimensional silicon strip detector (exposure time: 1 h (binary) and 1-4 h (ternary)). A binary Mn-Rh sample (34 at.% Rh) was analyzed by high temperature XRD under vacuum, using an Anton Paar XRK 900 reactor chamber on a Bruker D8 Advance Diffractometer. For evaluation and Rietveld refinement of all diffraction patterns the TOPAS® 4.2 software[35] was used.

4 Results and Discussion

A total of 27 ternary Bi–Mn–Rh and nine binary Mn-Rh samples were prepared and investigated. The results of XRD and EDX measurements (listed together with experimental information in Table 2) were used to construct the binary phase diagram and isothermal sections at 330 °C and 600 °C respectively. DTA results of binary Mn-Rh samples are summarized in Table 3. EDX area scans were used to determine the composition of the matrix solidified from the liquid during quenching, especially in the 600 °C section, which has been denoted by "solidified liquid = L" in Table 2.

4.1 Binary Mn-Rh Phase Diagram

In Fig. 1 the partial Mn-Rh phase diagram up to 90 at.% Rh, based on obtained as well as on literature data[15,26,27,33] is presented. Figure 2 shows the lattice parameter a of γ'-Mn$_3$Rh as a function of the Rh

Table 2 Experimental phase composition and lattice parameters of phases in the selected samples annealed at 600 and 330 °C, respectively

Nominal composition (at.%)	Heat treatment (d/°C)	XRD			EDX		
		Phase	Lattice parameters Å	deg (°)	Bi (at.%)	Mn (at.%)	Rh (at.%)
$Mn_{40}Rh_{60}$	10/600[c]	Rh	$a = 3.806\ (3)$	...	...	25.4	74.6
		MnRh (cubic)	$a = 3.043\ (7)$	...	...	51.2	48.8
$Mn_{60}Rh_{40}$	14[d]	MnRh (tetragonal)	$a = 2.770\ (2)\ c = 3.631\ (5)$	...	–	–	–
$Mn_{66}Rh_{34}$	1/320[g]	Rh^{i}	$a = 3.811\ (6)$	...	...	0.0	100.0
		MnRh (cubic)	$a = 3.049\ (8)$	...	...	66.1	33.9
$Mn_{67}Rh_{33}$	14/600[c]	γ'-Mn_3Rh	$a = 3.828\ (8)$	...	...	...	...
$Mn_{70}Rh_{30}$	10/600[c]	γ'-Mn_3Rh	$a = 3.821\ (4)$	...	...	...	–
$Mn_{75}Rh_{25}$	10/600[c]	γ'-Mn_3Rh	$a = 3.815\ (6)$	...	...	...	...
$Mn_{80}Rh_{20}$	10/600[c]	γ'-Mn_3Rh	$a = 3.805\ (5)$	...	...	...	...
$Mn_{85}Rh_{15}$	10/600[c]	γ'-Mn_3Rh	$a = 3.801\ (2)$	...	...	84.1	15.9
		α-Mn	$a = 8.924\ (1)$	...	...	99.6	0.4
$Mn_{95}Rh_5$	12/600[c]	γ'-Mn_3Rh	$a = 3.801(2)$	...	–	85.2	14.8
		α-Mn	$a = 8.928\ (8)$	...	...	99.3	0.7
$Bi_{64.9}Mn_{9.9}Rh_{25.2}$	120/330[a]	α-Bi_2Rh	$a = 6.921\ (3)\ b = 6.793\ (7)$ $c = 6.961\ (5)$	$\alpha = 117.73(2)$	64.5	0.3	35.2
		Bi_4Rh	$a = 14.926(8)$	...	78.5	0.1	21.4
		$Bi_{18}Mn_5Rh_6$	$a = 18.500(6)\ c = 4.160\ (4)$	...	60.6	17.2	22.2
$Bi_{73.9}Mn_{10}Rh_{16.1}$	120/330[a]	$L(Bi)^{f}$	$a = 4.547\ (5)\ c = 11.862(3)$	...	98.3	1.7	0.0
		Bi_4Rh	$a = 14.919(4)$	...	78.8	0.0	21.2
		$Bi_{18}Mn_5Rh_6$	$a = 18.493(2)\ c = 4.163\ (5)$	...	61.8	16.8	21.4
$Bi_{49}Mn_{11.8}Rh_{39.2}$	120/330[a]	Rh	$a = 3.802\ (2)$	...	1.1	0.1	98.8
		BiRh	$a = 4.097\ (6)\ b = 5.668\ (1)$	...	48.4	0.2	51.4
		α-Bi_2Rh^{e}	$a = 6.920\ (1)\ b = 6.794\ (1)$ $c = 6.962\ (1)$	$\alpha = 117.72(2)$	64.1	0.3	35.6
$Bi_{74.5}Mn_{15.5}Rh_{10}$	120/330[a]	$Bi_{18}Mn_5Rh_6$	$a = 18.528(8)\ c = 4.163(6)$	...	–	0.2	0.0
		$L(Bi)^{f}$	$a = 4.547(4)\ c = 11.863(3)$	...	99.8	0.2	0.0
		$Bi_4Mn_5Rh_2$	$a = 12.290(4)$	...	36.0	44.4	19.6
		Bi_3MnRh	$a = 8.853\ (6)\ b = 13.675(3)\ c = 4.129\ (5)$	...	58.4	20.0	21.6
$Bi_{58}Mn_{19}Rh_{23}$	120/330[a]	$Bi_xMn_{1-x}Rh$	$a = 3.060\ (1)$	...	3.6	51.7	44.7
		$Bi_{18}Mn_5Rh_6$	$a = 18.494(4)\ c = 4.163\ (2)$	...	60.8	17.2	22.0

Table 2 continued

Nominal composition (at.%)	Heat treatment (d/°C)	XRD			EDX		
		Phase	Lattice parameters		Bi (at.%)	Mn (at.%)	Rh (at.%)
			Å	deg (°)			
$Bi_{65.1}Mn_{19.9}Rh_{15}$	$120/330^a$	$L(Bi)^f$	$a = 4.547\,(4)\ c = 11.863(2)$	...	100.0	0.0	0.0
		Bi_3MnRh	$a = 8.852\,(2)\ b = 13.675(2)$ $c = 4.129(4)$	...	59.2	19.4	21.4
		$Bi_4Mn_5Rh_2$	$a = 12.290(3)$	...	35.9	45.0	19.1
$Bi_{65.0}Mn_{29.9}Rh_{5.1}$	$120/330^a$	$L(Bi)^f$	$a = 4.546\,(7)\ c = 11.862(1)$	...	97.1	2.9	0.0
		$\gamma'\text{-}Mn_3Rh$	$a = 3.813\,(1)$	...	0.6	76.7	22.7
		$BiMn_{1.05}Rh_{0.02}$	$a = 8.671\,(4)\ b = 47.639(4)$ $c = 15.019(5)$	...	48.9	49.7	1.4
$Bi_{49.4}Mn_{30.4}Rh_{20.2}$	$120/330^a$	Bi_3MnRh	$a = 8.851(2)\ b = 13.676(3)$ $c = 4.128\,(3)$	...	58.7	19.5	21.8
		$Bi_4Mn_5Rh_2$	$a = 12.289(1)$	...	36.0	44.7	19.3
$Bi_{50}Mn_{48}Rh_2$	$120/330^b$	$L(Bi)^f$	$a = 4.547\,(6)\ c = 11.859(3)$	...	97.7	2.3	0.0
		$\gamma'\text{-}Mn_3Rh^h$	$a = 3.812\,(4)$	...	0.4	77.4	22.2
		$BiMn_{1.05}Rh_{0.02}$	$a = 8.672\,(6)\ b = 47.654(7)$ $c = 15.023(1)$	...	49.2	49.6	1.2
$Bi_{27.6}Mn_{51.3}Rh_{21.1}$	$120/330^a$	$\alpha\text{-}BiMn$	$a = 4.289\,(3)\ c = 6.118\,(2)$	...	–	–	–
		$\gamma'\text{-}Mn_3Rh$	$a = 3.812\,(4)$	...	0.0	76.0	24.0
		Bi_3MnRh	$a = 8.850(5)\ b = 13.678(7)$ $c = 4.129(3)$	...	58.6	19.5	21.9
		$Bi_4Mn_5Rh_2$	$a = 12.289(2)$	...	35.6	45.4	19.0
		$BiMn_{1.05}Rh_{0.02}^e$	$a = 8.680\,(3)\ b = 47.688(8)$ $c = 15.021(4)$	...	50.6	48.3	1.1
		$Bi_{18}Mn_5Rh_6^e$	$a = 18.493(8)\ c = 4.164\,(3)$	...	–	–	–
$Bi_{16.9}Mn_{68.3}Rh_{14.8}^*$	$120/330^a$	$\alpha\text{-}Mn$	$a = 8.913\,(2)$	...	0.2	99.8	0.0
		$\gamma'\text{-}Mn_3Rh$	$a = 3.812\,(5)$	...	0.1	76.3	23.6
		$BiMn_{1.05}Rh_{0.02}$	$a = 8.673\,(4)\ b = 47.697(1)$ $c = 15.039(6)$	...	48.5	50.8	0.7
		Bi_3MnRh^e	$a = 8.857\,(2)\ b = 13.675(3)$ $c = 4.121\,(7)$	...	–	–	–
		Rh^i	–	...	0.0	100	0.0

Table 2 continued

Nominal composition (at.%)	Heat treatment (d/°C)	XRD			EDX		
		Phase	Lattice parameters Å	deg (°)	Bi (at.%)	Mn (at.%)	Rh (at.%)
$Bi_{64.5}Mn_{10.3}Rh_{25.2}$	$120/600^a$	$L(Bi)^f$	$a = 4.547(7)\ c = 11.867(7)$	…	87.5	0.5	11.9
		$\beta\text{-}Bi_2Rh$	$a = 6.741(4)\ b = 7.058(9)\ c = 7.071(9)$	$\alpha = 104.82(3)\ \beta = 100.80(5)\ \gamma = 105.81(2)$	65.2	0.1	34.7
		$\beta\text{-}MnRh(Bi)$	$a = 3.105(7)$	…	9.3	39.0	51.7
$Bi_{48.7}Mn_{10.3}Rh_{41}$	$120/600^a$	$BiRh$	$a = 4.086(1)\ c = 5.671(2)$	…	47.3	0.1	52.6
		$\beta\text{-}Bi_2Rh$	$a = 6.740(2)\ b = 7.027(3)\ c = 7.059(3)$	$\alpha = 104.8(3)\ \beta = 100.7(4)\ \gamma = 105.8(7)$	66.4	0.0	33.6
$Bi_{23}Mn_{13}Rh_{64}$	$24/600^b$	$\beta\text{-}MnRh(Bi)$	$a = 3.114(3)$	…	10.5	37.7	51.8
		Rh	$a = 3.806(3)$	…	1.4	1.1	97.5
		$BiRh$	$a = 4.097(3)\ c = 5.668(6)$	…	48.2	0.4	51.4
$Bi_{65}Mn_{15}Rh_{20}$	$24/600^b$	$\beta\text{-}MnRh(Bi)$	$a = 3.118(1)$	…	11.0	38.0	51.0
		$L(Bi)^f$	$a = 4.547(9)\ c = 11.863(3)$	…	97.8	2.2	0.0
		$\beta\text{-}MnRh(Bi)$	$a = 3.089(4)$	…	6.7	46.3	47.0
		$Bi_{18}Mn_5Rh_6^f$	$a = 18.542(9)\ b = 4.182(3)$	…	62.1	16.3	21.6
$Bi_{74.5}Mn_{15.4}Rh_{10.1}$	$120/600^a$	$L(Bi)^f$	$a = 4.547(3)\ c = 11.864(8)$	…	99.7	0.3	0.0
		$\beta\text{-}MnRh(Bi)$	$a = 3.058(3)$	…	0.6	55.6	43.8
		$Bi_4Mn_5Rh_2^f$	$a = 12.292(6)$	…	35.1	43.8	21.1
$Bi_{39}Mn_{19}Rh_{42}$	$24/600^a$	$\beta\text{-}Bi_2Rh$	$a = 6.738(2)\ b = 7.024(3)\ c = 7.057(3)$	$\alpha = 104.76(2)\ \beta = 100.75(4)\ \gamma = 105.74(2)$	64.9	0.0	35.1
		$\beta\text{-}MnRh(Bi)$	$a = 3.112(5)$	…	9.7	39.4	50.9
$Bi_{74}Mn_{20.3}Rh_{5.7}$	$120/600^a$	$L(Bi)^f$	$a = 4.547(3)\ c = 11.864(1)$	…	97.9	2.1	0.0
		$BiMn_{1-x}Rh_x^f$	$a = 5.955(3)\ b = 4.337(3)\ c = 7.491(6)$	…	48.4	50.1	1.5
		$Bi_4Mn_5Rh_2^f$	$a = 12.298(8)$	…	34.9	44.4	20.7
$Bi_{60}Mn_{26.5}Rh_{13.5}$	$24/600^b$	$L(Bi)^f$	$a = 4.547(3)\ c = 11.863(1)$	…	97.5	2.5	0.0
		$\beta\text{-}MnRh(Bi)$	$a = 3.061(7)$	…	0.4	63.3	36.3
		$Bi_4Mn_5Rh_2^f$	$a = 12.295(3)$	…	37.1	45.2	17.7
		$BiMn_{1-x}Rh_x^f$	$a = 5.955(6)\ b = 4.333(4)\ c = 7.472(1)$	…	49.0	49.9	1.1
$Bi_{50}Mn_{29.9}Rh_{20.1}$	$120/600^a$	$L(Bi)^f$	$a = 4.547(2)\ c = 11.864(6)$	…	98.9	1.1	0.0
		$\beta\text{-}MnRh(Bi)$	$a = 3.071(5)$	…	0.9	57.1	42.0
		Bi_3MnRh^f	…	…	58.0	18.7	23.3

Table 2 continued

Nominal composition (at.%)	Heat treatment (d/°C)	XRD			EDX		
		Phase	Lattice parameters		Bi (at.%)	Mn (at.%)	Rh (at.%)
			Å	deg (°)			
$Bi_{64.8}Mn_{30.2}Rh_5$	120/600[a]	$L(Bi)^f$	$a = 4.547(5)\ c = 11.865(3)$	...	99.7	0.3	0.0
		γ'-Mn_3Rh	$a = 3.813\ (7)$	...	0.4	74.9	24.7
		$BiMn_{1-x}Rh_x^f$	$a = 5.957\ (1)\ b = 4.339\ (2)$ $c = 7.506\ (4)$	...	49.2	49.8	0.0
$Bi_{47.5}Mn_{32.5}Rh_{20}$	24/600[b]	$L(Bi)^f$	$a = 4.547\ (3)\ c = 11.862(1)$	...	99.2	0.8	0.0
		β-$MnRh(Bi)$	$a = 3.058\ (3)$	...	0.2	60.4	39.4
		$Bi_{14}Mn_5Rh_2^f$	$a = 12.290(2)$	...	35.6	45.6	18.8
$Bi_{10}Mn_{38}Rh_{52}$	24/600[b]	Rh	$a = 3.807\ (1)$	...	0.0	22.0	78.0
		β-$MnRh(Bi)$	$a = 3.114\ (5)$	...	10.1	38.8	51.1
		$Bi_{18}Mn_5Rh_6^f$	$a = 18.558(1)\ b = 4.167(6)$	...	61.2	21.4	17.4
$Bi_{38.5}Mn_{47.5}Rh_{14}$	24/600[b]	$L(Bi)^f$	$a = 4.547(4)\ c = 11.863(2)$	...	98.6	1.4	0.0
		γ'-Mn_3Rh	$a = 3.814\ (2)$	...	0.3	73.1	26.6
		$BiMn_{1-x}Rh_x^f$	$a = 5.961\ (4)\ b = 4.341\ (4)$ $c = 7.503\ (8)$	...	45.5	53.9	0.6
$Bi_{30}Mn_{50}Rh_{20}$	120/600[a]	$L(Bi)^f$	$a = 4.547\ (5)\ c = 11.865(2)$	...	97.3	2.7	0.0
		γ'-Mn_3Rh	$a = 3.813\ (6)$	...	0.4	72.8	26.8
		β-$MnRh(Bi)$	$a = 3.074\ (6)$	...	0.4	63.4	36.2
		$BiMn_{1-x}Rh_x^f$	$a = 5.950\ (7)\ b = 4.342\ (9)$ $c = 7.504\ (2)$	...	48.3	50.9	0.8
$Bi_{31}Mn_{57}Rh_{12}$	24/600[b]	α-Mn	$a = 8.927\ (1)$	...	0.0	100.0	0.0
		$L(Bi)^f$	$a = 4.547\ (4)\ c = 11.862(4)$	...	100.0	0.0	0.0
		γ'-Mn_3Rh	$a = 3.809\ (3)$	...	0.2	75.9	23.9
		$BiMn_{1-x}Rh_x^f$	$a = 5.807\ (4)\ b = 4.337\ (4)$ $c = 7.545\ (7)$	...	48.2	51.5	0.3
$Bi_{17}Mn_{68}Rh_{15}$	120/600[a]	α-Mn	$a = 8.935\ (2)$	...	0.0	100.0	0.0
		$L(Bi)^f$	$a = 4.547\ (6)\ c = 11.864(3)$	...	98.4	1.6	0.0
		γ'-Mn_3Rh	$a = 3.809\ (6)$	...	0.3	77.9	21.8
		$BiMn_{1-x}Rh_x^f$	$a = 5.808\ (1)\ b = 4.375\ (6)$ $c = 7.499\ (8)$	...	48.5	50.5	1.0

[a,b,c,d]Preparation method (refer to the text): [a]Sintered pellet; [b]Powder pellet in alumina crucible, [c]Arc melting, [d]Arc melting and slowly cooled to room temperature after annealing at 320 °C for 14 days (not marked in Fig. 1); [e]Traces of non-equilibrium phases; [f]Solidified liquid (please refer to text); [g]Sample was annealed for 21 days at 320 °C, manually pulverized in liquid N_2 afterwards stress annealed for 24 h and quenched in cold water; [h]Non-equilibrium minority phase present with < 10 wt% in XRD; [i]Traces of unreacted pure metals; *Phase not marked in Fig. 6

Table 3 Summary of measured thermal effects of selected binary and ternary samples

Nominal composition (at.%)	Heat treatment (d/°C)	Thermal effects		
		Heating (°C)	Cooling (°C)	
			Other	Transition
$Mn_{67}Rh_{33}$	14/600	426, 509	338	871
$Mn_{70}Rh_{30}$	10/600	590[a]	…	911
$Mn_{75}Rh_{25}$	10/600	587[a]	…	920
$Mn_{80}Rh_{20}$	10/600	560[a]	…	818
$Bi_{50}Mn_{48}Rh_2$	21/330	260, 423	…	…

[a]Magnetic transition
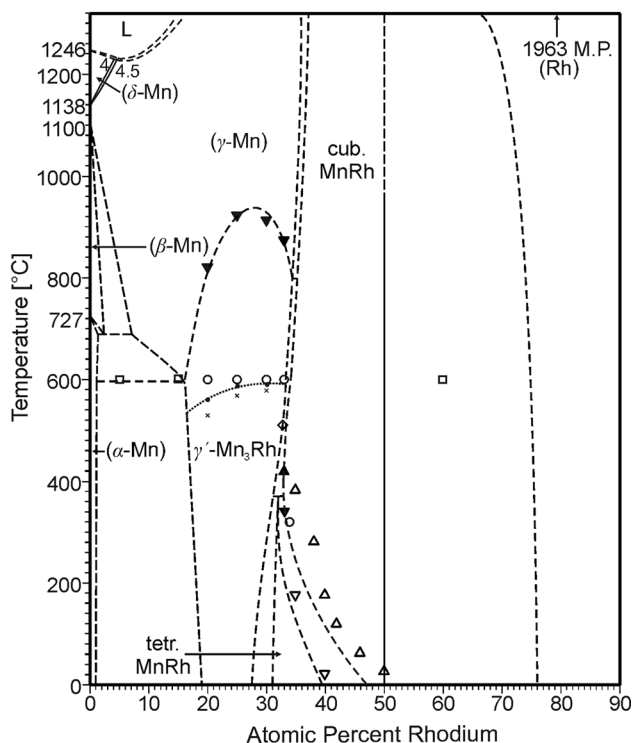
Fig. 1 Mn-Rh phase diagram according to the present results and literature data.[15,26,27,33] Dashed lines are estimated; circle (○ single phase) and square (□ two phase): nominal compositions of the respective samples; inverted filled triangles (▼): transition temperature of ordered γ'-Mn_3Rh to γ-Mn solid solution respectively tetragonal to cubic MnRh phase; open (△) and open inverted (▽) triangles: temperature hysteresis at the transition from the tetragonal to cubic MnRh structure[26]; filled circles: (●) magnetic transition observe by DTA measurements; crosses (x): Néel temperature of ordered alloys[33]; open squares (□): transition temperature from two phase field (tetragonal + cubic MnRh phase) to the single phase field γ'-Mn_3Rh. Please refer to the text

concentration compared with values from literature[16,31,34] whereas a XRD pattern of a sample containing 15 at.% Rh is given in Fig. 3 and the high temperature XRD patterns of a sample with 34 at.% Rh in Fig. 4. A detailed discussion of the assessed phase equilibria is given below.

4.2 Composition Range 0-17 at.% Rh

In the previously published diagram[15] the two phase field of α-Mn and γ'-Mn_3Rh ranges from 1-13 at.% Rh at 400 °C and 1-11 at.% Rh at 600 °C, however XRD data suggests the coexistence of both phases in a sample containing 15 at.% Rh (annealed at 600 °C, Fig. 3). A graphical interpolation of the lattice parameter a of γ'-Mn_3Rh (Fig. 2) at 600 °C indicates the border of the two phase field (α-Mn + γ'-Mn_3Rh) at the γ'-Mn_3Rh phase at 16.7 at.% Rh. The results are also different to a study of Yamauchi et al.,[31] where the authors show XRD patterns of disordered γ-MnRh samples between 8 and 14 at.% Rh without any α-Mn reflexes.

4.3 γ'-Mn_3Rh Phase

The obtained homogeneity range of the γ'-Mn_3Rh phase differs from data reported in the literature,[15] and the transition temperature from ordered γ'-Mn_3Rh phase to the γ-Mn solid solution also shows deviations between this work and previous literature.

A graphical interpretation of the DTA values indicates a maximum of the transition temperature around 940 °C between 25 and 30 at.% Rh (Fig. 1). This is approximately 80 °C higher as reported.[15,16] Due to the better evaluability of the cooling effects on the higher order transition, only the cooling temperatures are given in Fig. 1 and Table 3. Thermal effects between 560 °C (20 at.% Rh) and 590 °C (30 at.% Rh) observed in DTA measurements are probably associated with a magnetic transition. Albeit this DTA effects appear slightly higher than reported in References [33–36], the described correlation of increasing Néel temperature with larger Rh concentrations is confirmed.

The present results of the homogeneity range of the ordered γ'-Mn_3Rh phase, which are based on lattice parameter investigations, are also in significant contrast to the reported values, particularly in Reference [15,16,27,30,32] E. Raub and Mahler,[16] who annealed their samples at

Fig. 2 Lattice parameter a in γ'-Mn$_3$Rh as a function of the Rh concentration. The dashed line indicates the proposed phase boundary at 600 °C
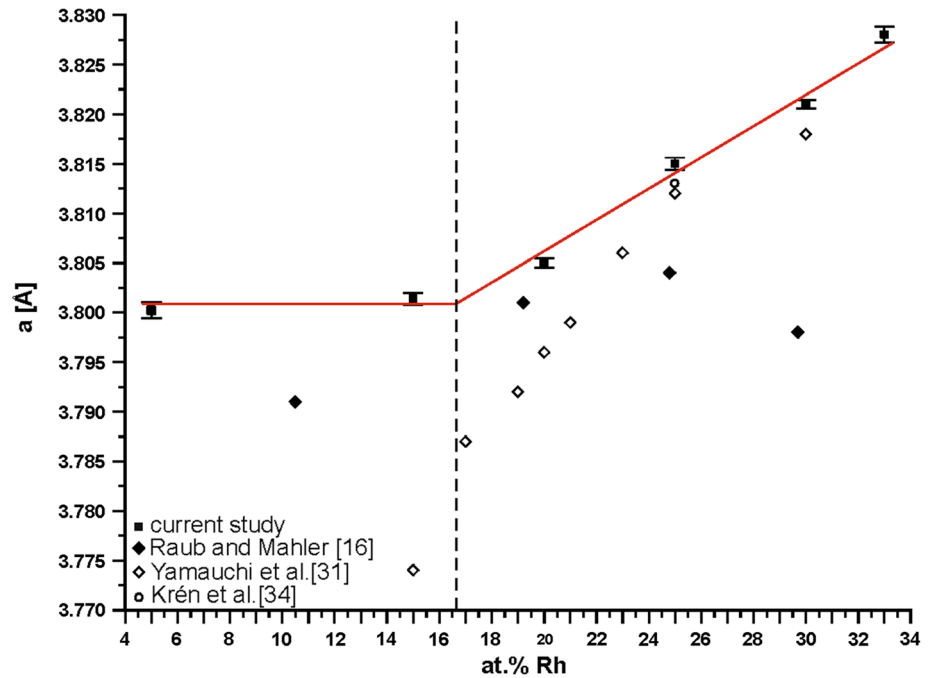
different temperatures, determined the homogeneity range from 11 to 32 at.% Rh at 600 °C. Selte et al.[27] show the Rhodium-rich composition limit at $\sim$ 27 at.% Rh.

As described before, the evaluation of lattice parameter a indicates that at 600 °C the phase boundaries are ranging from 16.7 to more than 33 at.% Rh. The obtained lattice parameters are in a good agreement with those given in References [32–34], particularly at the stoichiometric composition with a = 3.815(6) Å. The values by Yamauchi et al.[32] are slightly lower, especially at lower Rh concentrations.

4.4 Two Phase Field γ'-Mn$_3$Rh + β-MnRh and the Tetragonal to Cubic MnRh Phase Transition

The compilation[15] shows phase boundaries without temperature dependence between 32 and 35 at.% Rh (γ'-Mn$_3$-Rh respectively γ-Mn + β-MnRh). In contrast to this, results of our sample with 33 at.% Rh, and data by Selte et al.[27] indicate a meandering phase field with a spread towards lower temperatures. XRD measurement of our sample at 33 at.% Rh shows the exclusive existence of the γ'-Mn$_3$Rh phase (lattice parameter a = 3.828(8) Å) at 600 °C. DTA analyses show in first and second heating's an endothermic effect at $\sim$ 426 °C and the corresponding cooling effect at $\sim$ 338 °C. These effects are connected with the entrance to the single cubic MnRh phase field (heating) and the crystallisation of the tetragonal MnRh (cooling).

The effect end at 509 °C represents probably the entrance to the γ'-Mn$_3$Rh single-phase field. The transition to the γ-Mn phase appears at 871 °C. These data suggest that the two-phase field between MnRh and γ'-Mn$_3$Rh (γ-Mn) is shifted to higher Rh contents at higher temperature. In study,[27] the range of the two-phase field at room temperature is reported between 28 and 31 at.% Rh with a trend towards a broader field at lower temperatures. These values are accepted in our phase diagram shown in Fig. 1.

A sample with 40 at.% Rh, annealed at 320 °C slowly cooled down to room temperature and manually pulverized in liquid N$_2$, contains only the tetragonal MnRh phase with a lattice parameters of a = 2.770(2) Å, c = 3.631(5) Å, V = 27.855(5) A^3. These values are in a good agreement to data reported by Selte et al.,[27] who show in their figures lattice parameters a = 2.768 Å, c = 3.633 Å, V = 27.83 A^3, of a sample quenched from over 500 °C. A further sample, containing 34 at.% Rh annealed for 21 days at 320 °C slowly cooled down to room temperature and manually pulverized in liquid N$_2$, was subjected to a high temperature XRD measurement for a better understanding of the phase transition between the tetragonal and the cubic MnRh phase. After manual pulverization in liquid N$_2$ the powder was stress annealed for 24 h at 320 °C. Unexpectedly, the cubic MnRh phase was exclusively found and no tetragonal MnRh phase was present at this temperature (Fig. 4; bottom). This suggests, that at 34 at.% Rh and 320 °C the sample is situated in the cubic MnRh single phase field. The high temperature XRD measurement was carried out with not stress-annealed powder (Fig. 4 (top)), leading to very wide reflections. This complicates

292

J. Phase Equilib. Diffus. (2020) 41:282–298
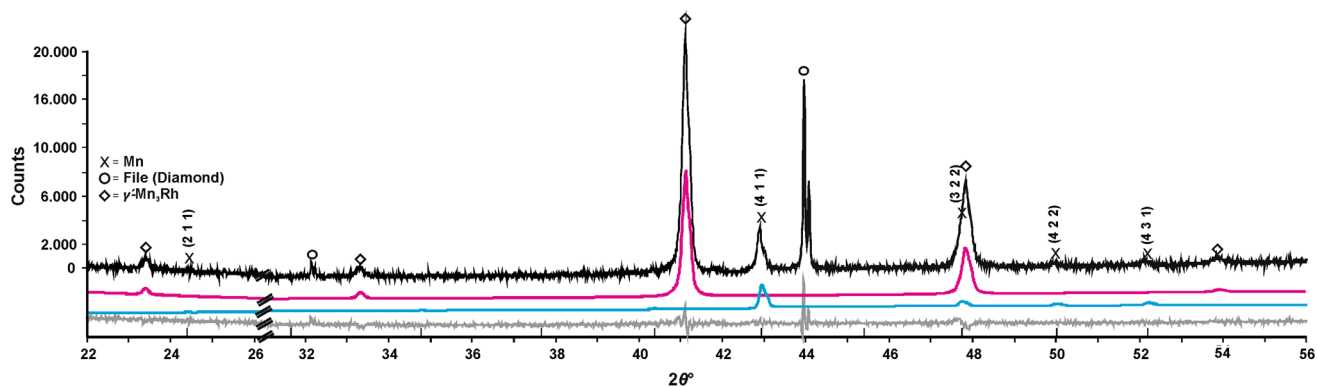
Fig. 3 Powder XRD pattern of the sample $Mn_{85}Rh_{15}$ (annealed and stress annealed at 600 °C), measured at ambient conditions. The pattern contains the two phases γ'-Mn_3Rh, α-Mn and contaminants of the diamond file. The experimental pattern (above), the calculated pattern of the γ'-Mn_3Rh phase and α-Mn middle and the difference curve (bottom) are shown. Miller indices are given for the first α-Mn reflexes
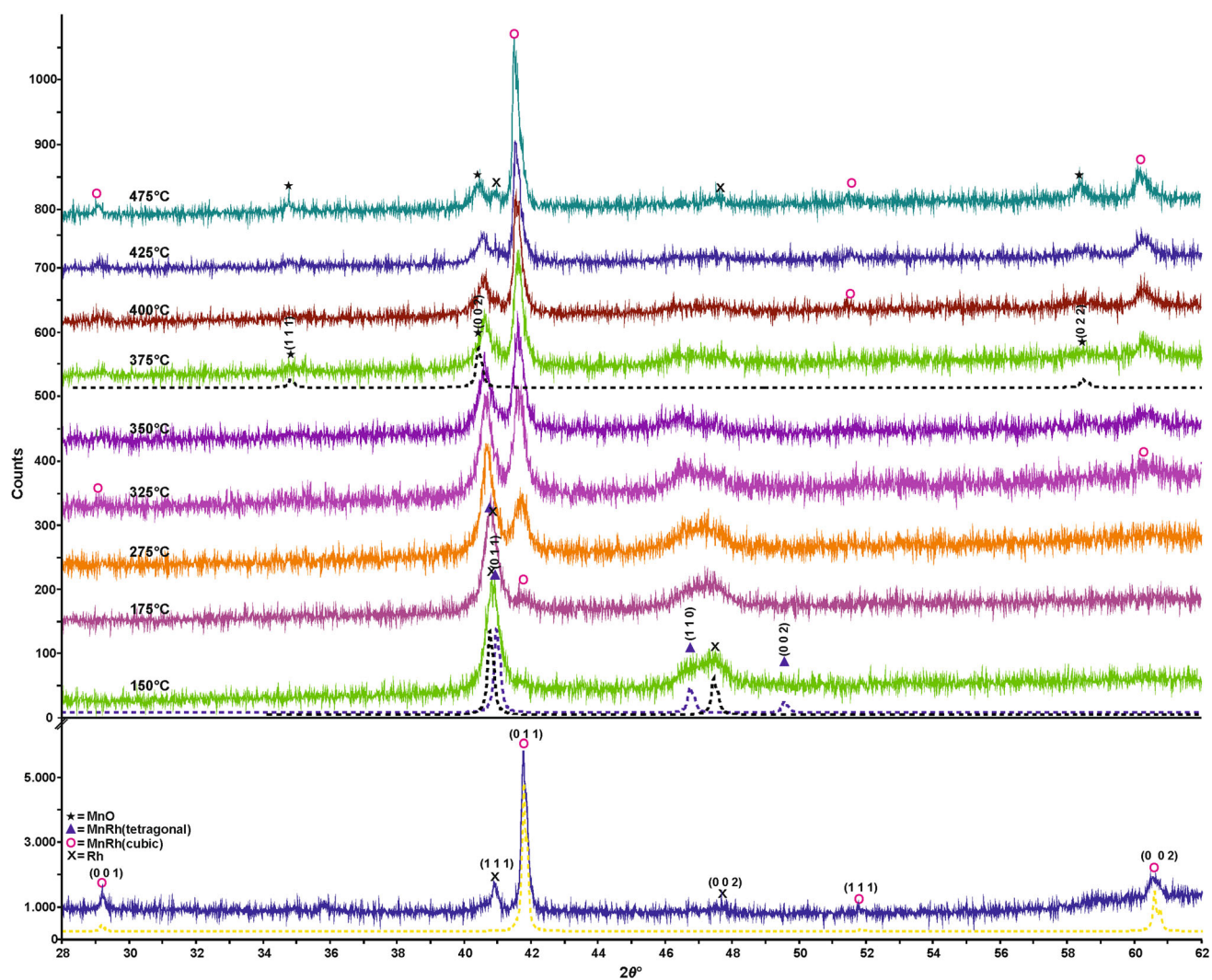
Fig. 4 Powder XRD pattern of a sample with 34 at.% Rh slowly cooled down from 320 °C, measured at different temperatures (top) and 24 h stress annealed at 320 °C, measured at ambient conditions (bottom). The dashed lines show the calculated XRD reflexes cubic MnRh; Rh, tetragonal MnRh (150 °C) and MnO (375 °C). The refinement is based on the structures given by Ref. [25,38,39] Values in brackets are Miller indices

distinguishing the (011) main reflex of the tetragonal MnRh phase and the (111) Rh reflex, arising of not reacted base material, appearing around 40.8 $2\theta°$. The same situation also applies with the (110) tetragonal MnRh phase and (002) Rh reflex around 47 $2\theta°$ at 150 °C. Nevertheless it can be clearly seen that the (011) main reflex of the cubic MnRh phase at 41.6 $2\theta°$ firstly appears at 175 °C. At 325 °C also the (001) 29.8 $2\theta°$ and (002) 60.3 $2\theta°$ cubic MnRh reflexes are identifiable. Towards the 400 °C measurement, the (011) and more cognizable the (110) reflexes of the tetragonal MnRh are still existent at 375 °C. These tetragonal MnRh reflexes disappear completely at 400 °C and only the cubic MnRh reflexes can be identified. The MnO reflexes appearing at 375 °C are due to leakage problems of the reaction camber.

The observations are in good agreement with the DTA data. The first emerging of the cubic MnRh reflexes and the slow disappearing of tetragonal MnRh above temperature of 300 °C confirms the big hysteresis reported in Reference [26] suggesting slow kinetics of the phase transformation. We conclude, that cubic MnRh is formed between 150 and 175 °C in our sample and that the presence of tetragonal MnRh above 320 °C is due to kinetic effects and does not represent the equilibrium. The phase boundaries of cubic and tetragonal MnRh are drawn dashed in this region, reflecting the rather high uncertainty in this area.

4.5 Two Phase Field MnRh + Rh

A sample containing 60 at.% Rh (annealed at 600 °C) shows both phases, Rh ($a = 3.806(3)$ Å) and cubic MnRh ($a = 3.043(7)$ Å) in equilibrium. These values are in very good agreement with literature,[16] wherein $a = 3.808$ Å (Rh) and $a = 3.040$ Å (cubic MnRh) were reported for the same sample composition, although the sample was annealed at 800 °C. The cubic MnRh lattice parameter matches also perfect with values given in Reference [27] where a constant a value of 3.043 Å for sample between 50 and 56 at.% Rh is reported.

EDX results of the latter sample revealed a composition of the cubic MnRh phase of 51.2 at.% Rh, and a solubility of 25.4 at.% Mn in Rh. It can be derived that the two phase field ranges from $\sim$ 51 to $\sim$ 75 at.% Rh at 600 °C, which is also in perfect agreement with the phase boundaries reported by References [16] and [27].

4.6 The BiMn$_{1-x}$Rh$_x$ Phase

Concomitant with the disputation of the crystal structure (see Chap. 2.1.) of β-BiMn, also the crystal structure of Rh stabilised β-BiMn is not fully understood. There are two models: BiMn$_{1.05}$Rh$_{0.02}$[11] and BiMn$_{1.1-x}$Rh$_x$[10] with x = 0.02 on the octahedral side.

A careful refinement of XRD power patterns of samples annealed and quenched from 330 °C (see e.g. Fig. 5), showed that the model BiMn$_{1.05}$Rh$_{0.02}$ fitted better than the BiMn$_{1.1-x}$Rh$_x$ model. In all samples annealed at 600 °C and quenched, however, the BiMn$_{1.1-x}$Rh$_x$ model leads to a better refinement. The latter phase, however, is formed from the liquid on quenching. Therefore, the refinement of XRD pattern from all 600 °C samples in this study was started by applying the setting of β-BiMn given in Reference [22], with a mixed occupancy of the Wyckoff position 2(d) from Mn/Rh = 0.98/0.02. This phase is hereinafter denoted as BiMn$_{1-x}$Rh$_x$ (Tables 1 and 2).

Albeit their massy appearance combined with the morphology of a sharp-edged and elongated habitus of several µm (Fig. 9(a); Bi$_{64.8}$Mn$_{30.2}$Rh$_5$) in several ternary 600 °C
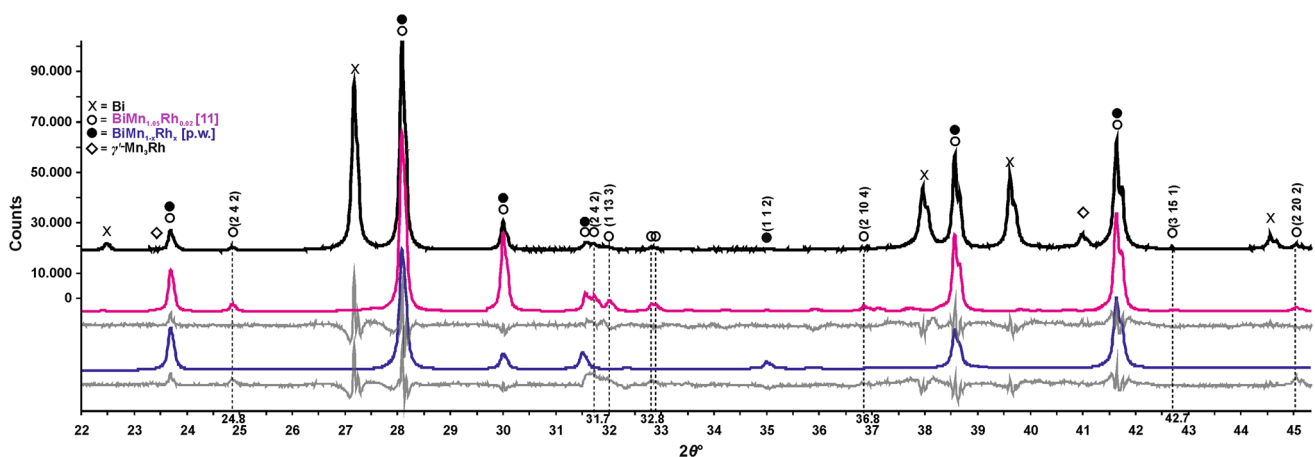
Fig. 5 Powder XRD pattern of the sample Bi$_{65.0}$Mn$_{29.9}$Rh$_{5.1}$ (annealed at 330 °C, measured at ambient conditions). The pattern contains Bi, γ'-Mn$_3$Rh and BiMn$_{1.05}$Rh$_{0.02}$. The experimental pattern (above, black), the calculated pattern of the phases BiMn$_{1.05}$Rh$_{0.02}$[11] (magenta middle) and BiMn$_{1-x}$Rh$_x$ (dark blue bottom) [p.w.] are shown. The grey lines below the calculated pattern are the difference curve of the corresponding refinement. Values in brackets are the Miller indices
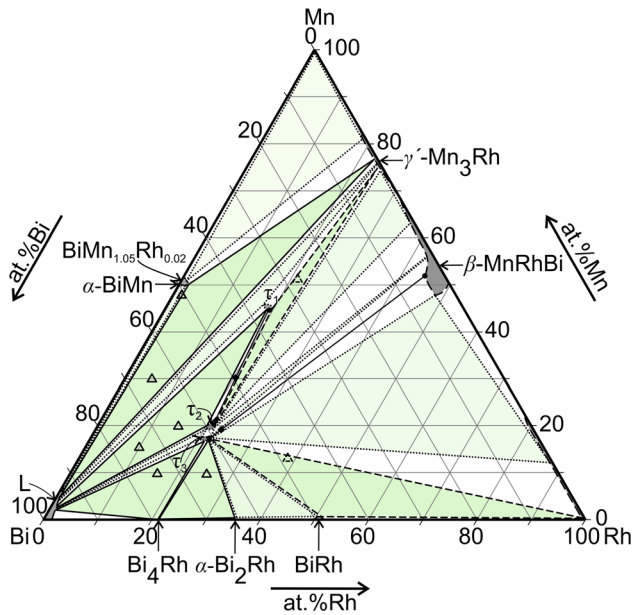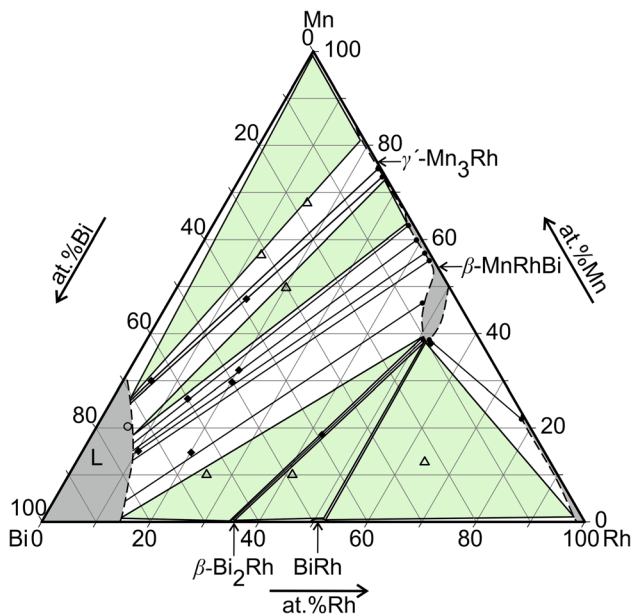
Fig. 6 Isothermal section at 330 °C; open data symbols indicate the nominal compositions of the respective samples, triangles (△): three-phase samples; filled squares (◆): two-phase samples; filled circles: (●) phase compositions measured with SEM/EDX; corresponding to Table 2: $\tau_1 = Bi_4Mn_5Rh_2$, $\tau_2 = Bi_3MnRh$, $\tau_3 = Bi_{18}Mn_5Rh_6$, cubic MnRh = β-MnRh(Bi)

Fig. 7 Isothermal section at 600 °C; open symbols indicate the nominal compositions of the respective samples, circles (○): single phase samples; triangles (△): three-phase samples; filled squares (◆): two-phase samples; filled circles: (●) phase compositions measured with SEM/EDX; corresponding to Table 2: cubic MnRh = β-MnRh(Bi)

samples, the $BiMn_{1-x}Rh_x$ phases is only a quenching product and not an equilibrium phase. This is evidenced by a DTA determination of a sample with a composition of

$Bi_{50}Mn_{48}Rh_2$ (annealed at 330 °C) that shows two invariant reactions at 260 °C and 423 °C (Table 3). The reaction at 260 °C corresponds to the formation of the Bi-rich liquid (probably eutectic) and the second one at 423 °C to the decomposition of the $BiMn_{1.05}Rh_{0.02}$ phase. This decomposition is 23 °C lower than the peritectic decomposition of β-BiMn at 446 °C reported in Reference [15].

4.7 The Ternary Phase Diagram Bi–Mn–Rh

The isothermal sections at 330 °C and 600 °C, based on obtained data listed in Table 2, are shown in Figs. 6 and 7. Three-phase fields which were all confirmed by at least one sample are drawn using solid lines. Dashed lines indicate those phase fields only confirmed by samples showing local phase equilibrium but additional impurity phases due to sluggish equilibration. All phase equilibria that only arise from theoretical considerations and were not experimentally observed are indicated by dotted lines.

4.8 Isothermal Section at 330 °C

Due to synthesis difficulties based on different melting points of the elements and a slow reaction kinetic at low temperature on the Rh rich side, the isothermal section could only be investigated in the Bi-rich corner with more than 50 at.% Bi. Despite the long annealing time of 4 months all samples containing a higher amount of Rh or more than 50 at.% Mn are not in full equilibrium.

The isothermal section, shows 14 three-phase fields, of which four were fully confirmed experimentally. Additionally, the three-phase fields, (γ'-Mn_3Rh + τ_1+ τ_2) and (Rh + BiRh + τ_3) are confirmed by one sample each, however, at least one additional impurity phase, (marked with an "e" in Table 2) was determined by EDX and XRD analysis.

The three-phase field (α-Mn + γ'-Mn_3Rh + $BiMn_{1.05}Rh_{0.02}$) is also confirmed by one sample with a composition of $Bi_{16.9}Mn_{68.3}Rh_{14.8}$, would result in a graphical estimated phase boundary of ∼ 23 at.% Rh at the γ'-Mn_3Rh phase. Based on thermodynamic considerations the phase boundary of the ternary field would be expected close to the composition of the binary phase boundary at ∼ 17 at.% Rh (γ'-Mn_3Rh phase). For this reason and the additional presence of trace amounts of two other phases (non reacted Rh and Bi_3MnRh) in the bulk sample, the sample is not displayed in Fig. 1 and the three-phase field was indicated by dotted lines.

The three-phase field (L + α-BiMn + $BiMn_{1.05}Rh_{0.02}$) is confirmed by a sample ($Bi_{50}Mn_{48}Rh_2$) showing in XRD the mentioned phases and additionally also the γ'-Mn_3Rh (< 10 wt%) (Fig. 8). The occurrence of the four phases in a local equilibrium is based on the very close location of the

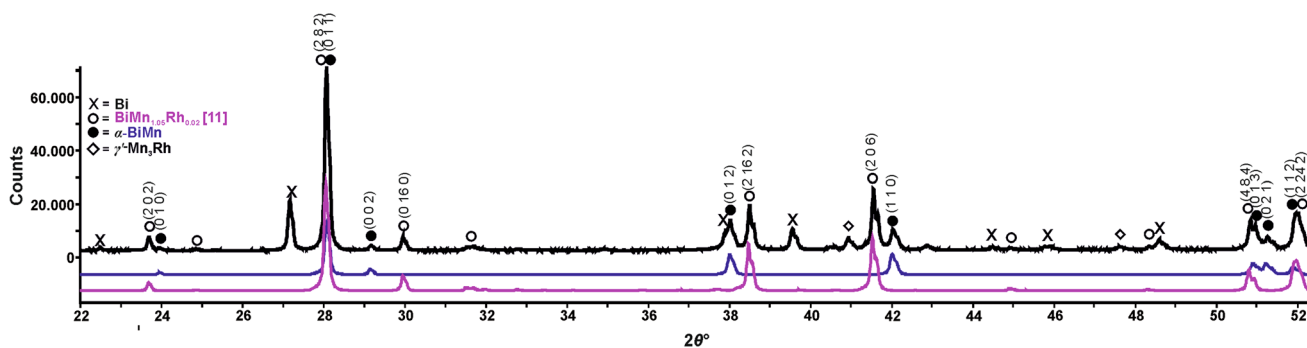J. Phase Equilib. Diffus. (2020) 41:282–298

295

Fig. 8 Powder XRD pattern of the sample $Bi_{50}Mn_{48}Rh_2$ (annealed at 330 °C, measured at ambient conditions). The pattern contains Bi, γ'-Mn_3Rh, $BiMn_{1.05}Rh_{0.02}$ and α-BiMn. The experimental pattern (above, black), the calculated pattern of the phases $BiMn_{1.05}Rh_{0.02}$[11] (magenta middle) and α-BiMn (dark blue bottom) are shown. Values in brackets are the Miller indices of the strongest reflexes

phase fields whereby the sample is situated on the border of the two three-phase fields. Another theoretical existing three-phase field, (α-BiMn + Mn + $BiMn_{1.05}Rh_{0.02}$), is not drawn due to the narrow space between the neighboring phase fields.

Except the reported three ternary phases ($Bi_4Mn_5Rh_2$ (τ_1)[13]; Bi_3MnRh (τ_2), $Bi_{18}Mn_5Rh_6$ (τ_3)[14]) and $BiMn_{1.05}Rh_{0.02}$, no further phases were found.

SEM studies indicated very limited ranges of Mn solubility (less than 0.5 at.% Mn) in all tree binary Bi-Rh compounds (Bi_4Rh, α-Bi_2Rh and BiRh). The EDX values in Table 2 differ somewhat from the stoichiometric compositions of 33.3 at.% Rh (α-Bi_2Rh) and 20 at.% Rh (Bi_4Rh). This discrepancy is due to problems with the WDX/EDX measurements: the characteristic XRD spectra of Bi and Rh, especially the Bi M-line at 2.419 keV and the Rh $L_{\alpha1}$ line at 2.697 keV, are rather close, which makes it difficult to separate them in the measurement. No hint, neither in XRD nor in EDX, could be found for Mn stabilization of the metastable phases Bi_3Rh or $BiRh_{0.81}$.[17]

The phase cubic MnRh (hereinafter denoted as β-MnRh(Bi) phase shows a measurable solubility of Bi into the ternary. Approximately 3.6 at.% Bi was found to replace Mn in the cubic MnRh structure in a sample composition of $Bi_{58}Mn_{19}Rh_{23}$. Whereby the lattice parameter $a = 3.060(1)$ Å is slightly higher compared with the unsubstituted cubic MnRh ($a = 3.044$ Å). These results are in agreement with Suits[12] who, reported a maximum substitution of 10 at.% Bi in β-MnRh(Bi) at 400 °C and a lattice parameter $a = 3.110$ Å. In contrast to the latter author, however, β-MnRh(Bi) was not found in equilibrium with BiRh. Instead the ternary τ_3 phase was found in equilibrium with $Bi_xMn_{1-x}Rh$. Suits[12] made his investigations at 400 °C, 70 °C higher than the current isothermal section, so a change of equilibria between these two temperatures is probable. In the 600 °C isothermal section discussed in the next section, a tie line exists between β-MnRh(Bi) and BiRh.

As described before, the α-BiMn phase appears (at 330 °C) only in a very small ternary area. Instead, the closely related orthorhombic compound $BiMn_{1.05}Rh_{0.02}$ described by Taufour et al.[11] is found in equilibrium with γ'-Mn_3Rh. In Tables 1 and 2 this phase name $BiMn_{1.05}Rh_{0.02}$ is used independently of the real Rh contend.

A sample with the composition $Bi_{65.0}Mn_{29.9}Rh_{5.1}$ (XRD pattern shown in Fig. 5, values given in Table 2), for example, contains (L(Bi) + γ'-Mn_3Rh + $BiMn_{1.05}Rh_{0.02}$) with composition for one phase of 48.9 at.% Bi, 49.7 at.% Mn, and 1.4 at.% Rh. This EDX result is in good agreement with the calculated phase formula by XRD data: $Bi_{48.48}Mn_{50.18}Rh_{1.34}$, but the Rh-content is slightly larger than suggested by the formula $BiMn_{1.05}Rh_{0.02}$. Except for the lattice parameter b, all parameters are equal to the values of[11] within the error limits.

4.9 Isothermal Section at 600 °C

The 600 °C isothermal section (Fig. 7) contains no ternary phase, so all of them are decomposing at temperatures between 330 and 600 °C. All five three-phase fields are experimentally confirmed. The four ternary phases ($Bi_4Mn_5Rh_2$, Bi_3MnRh, $Bi_{18}Mn_5Rh_6$ and also $BiMn_{1-x}Rh_x$) existing in the 330 °C isothermal section, occur in several different samples (marked with an "e" in Table 2). However, their morphology (e.g. Fig. 9(b)) indicates that they arise at the quenching process and are not equilibrium phases. According to the literature, the $Bi_4Mn_5Rh_2$ phase is stable up to 500 °C[13] and the $Bi_{18}Mn_5Rh_6$ phase up to 457 °C.[14] $BiMn_{1.05}Rh_{0.02}$ decomposes at 423 °C according to our DTA results.

Similar to the 330 °C section, EDX studies indicate a very limited Mn solubility (less than 0.4 at.% Mn) in all Bi-Rh compounds. Concluding from the two binary systems, the liquid phase field at the Bi corner is suggested to start at $\sim$ 69 at.% Bi on the Bi–Mn side, and to end at $\sim$ 85 at.% Bi and on the Bi-Rh side. However, all SEM/EDX

296

J. Phase Equilib. Diffus. (2020) 41:282–298

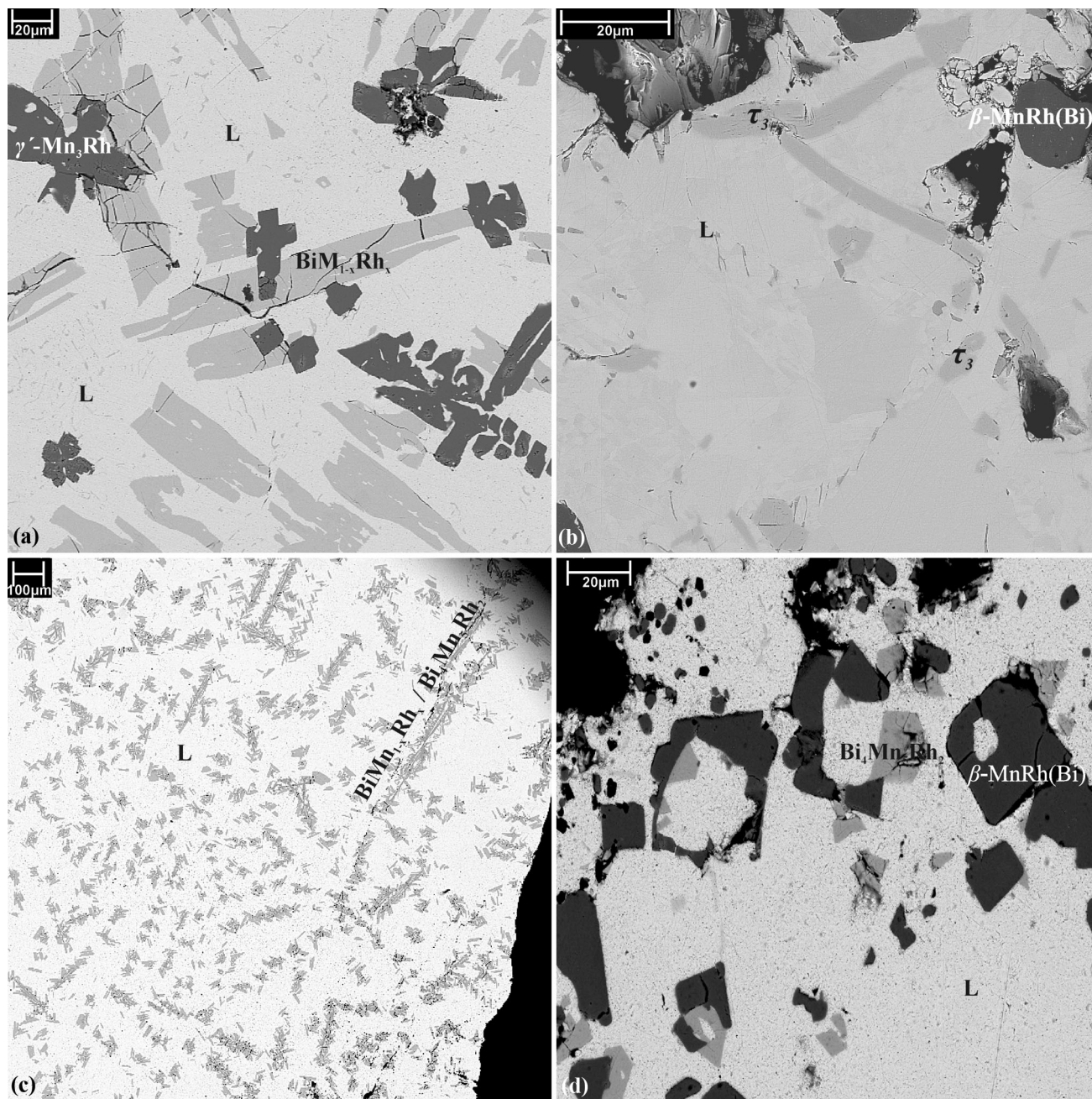**Fig. 9** SEM-BSE images of selected samples (black structures are either holes or cracks caused by sample preparation); (a) $Bi_{64.8}Mn_{30.2}$-Rh_5 (annealed at 600 °C), showing L (light gray) γ'-Mn_3Rh (dark) and $BiMn_{1-x}Rh_x$ (gray); (b) $Bi_{50}Mn_{29.9}Rh_{20.1}$ (annealed at 600 °C), showing L (light gray) β-MnRh(Bi) (dark gray) and Bi_3MnRh (τ_3) (gray); (c) $Bi_{75}Mn_{20.3}Rh_{5.7}$ (annealed at 600 °C), showing Bi (light gray) and interleaved $BiMn_{1-x}Rh_x/Bi_4Mn_5Rh_2$ (gray); (d) $Bi_{75}Mn_{20.3}$-$Rh_{5.7}$ (annealed at 600 °C), showing Bi (light gray) β-MnRh(Bi) (dark gray) and $Bi_4Mn_5Rh_2$ (gray)

measurements of samples containing L(Bi), except one ($Bi_{64.5}Mn_{10.3}Rh_{25.2}$), show a significantly lower Mn (≤ 3 at.%) and Rh (≤ 0.5 at.%) content for the quenched Bi-rich liquid phase as determined from area scans (Table 2). This would indicate a retrograde shape of the liquid phase field. On the other hand, the existence of rather large crystals of phases not stable at 600 °C clearly show,

that the quenching process is slow enough to allow for large and well-shaped crystallites.

The convex shape of the liquid phase boundary in the Bi-rich corner is deduced from the sample $Bi_{74}Mn_{20.3}Rh_{5.7}$. XRD analysis of the latter sample shows that beside Bi also the phases $BiMn_{1-x}Rh_x$ and $Bi_4Mn_5Rh_2$ are present with several wt%. Both phases are not stable at 600 °C, so it is

evident, that the sample was single phase Liquid at the time of annealing. The corresponding micrograph of the sample showing long needles of $BiMn_{1-x}Rh_x/Bi_4Mn_5Rh_2$ in a Bi matrix is shown in Fig. 9(c). The phase boundary of L in the 600 °C isothermal section was drawn to include this sample composition in the liquid single-phase region.

XRD and SEM investigations of the sample $Bi_{74.5}$-$Mn_{15.4}Rh_{10.1}$ (Fig. 9(d)) show beside L(Bi) also the phases β-MnRh(Bi) and $Bi_4Mn_5Rh_2$. Compared to sample Bi_{74}-$Mn_{20.3}Rh_{5.7}$ (Fig. 9(c)), where the phases $BiMn_{1-x}Rh_x$ and $Bi_4Mn_5Rh_2$ are formed during quenching, the morphology indicates that the β-MnRh(Bi) arises not at the quenching process and is an equilibrium phase, therefore the sample is outside liquid phase boundary.

Due to the problems to accurately measure the Mn- and Rh- content of the quenched liquid by area scans, the phase boundary itself is shown as a dashed line.

The β-MnRh(Bi) phase at 600 °C has a large solubility into the ternary field. Nearly 11 at.% Bi was found to replace Mn in cubic MnRh structure at a sample composition of $Bi_{23}Mn_{13}Rh_{64}$. A large substitution of Bi in the β-MnRh is in agreement with Suits,[12] who measured the maximum Bi content in a sample composition with 50 at.% Rh. This is confirmed in the current study. In general the data given in Table 2 indicate that the solubility of Bi is promoted by high Rh-contents around 50 at.%.

5 Conclusion

The Mn-Rh phase diagram in the range from 5 to 90 at.% Rh was reinvestigated by standard experimental methods, and a revised version is presented in Fig. 1. Based on the present results, the transition temperature from ordered γ'-Mn_3Rh phase to γ-Mn solid solution was reassessed. The phase fields, as reported by Massalski et al.,[15] could be confirmed although the phase boundary of the cubic MnRh phase had to be revised from 55 to 50 at.% Rh and the two-phase field of cubic MnRh + γ'-Mn_3Rh is much narrower than reported. A temperature hysteresis for the transformation from the tetragonal to the cubic MnRh structure given by Nakayama and Asanuma[26] could be confirmed.

In an attempt to stabilize the ferromagnetic phase α-BiMn by the addition of a third element, the ternary Bi–Mn–Rh phase diagram was investigated experimentally. Based on the results of thermal analyses, powder XRD, and SEM-EDX a large part of the ternary phase diagram could be elucidated. Two isothermal sections are shown: one at 330 °C, i.e. at a temperature below the peritectic decomposition of α-BiMn (Fig. 6), and a second at 600 °C.

References

1. M.J. Kramer, R.W. McCallum, I.A. Anderson, and S. Constantinides, Prospects for Non-Rare Earth Permanent Magnets for Traction Motors and Generators, *JOM*, 2012, **64**(7), p 752-763

2. M.C.J. Marker, P. Terzieff, P. Kainzbauer, M. Bobnard, K.W. Richter, and H. Ipser, BiMn: Synthesis Separation by Centrifugation, and Characterization, *J. Alloys Compd.*, 2018, **741**, p 682-688

3. Y. Liu, J. Zhang, G. Jia, Y. Zhang, Zh Ren, X. Li, Ch Jing, Sh Cao, and K. Deng, Magnetic Anisotropy Properties and Spin Reorientation for Textured Bi-Mn Alloys Fabricated by a Field-Inducing Technique, *Phys. Rev. B*, 2004, **70**, p 184424

4. N.V. Rama Rao, A.M. Gabay, and G.C. Hadjipanayis, Anisotropic Fully Dense MnBi Permanent Magnet with High Energy Product and Coercivity at Elevated Temperatures, *J. Phys. D*, 2013, **46**, p 062001

5. C. Cui, J.P. Choi, G. Li, E. Polikarpov, J. Darsell, N. Overman, M. Olszta, D. Schreiber, M. Bowden, T. Droubay, M.J. Kramer, N.A. Zarkevich, L.L. Wang, D.D. Johnson, M. Marinescu, I. Takeuchi, Q.Z. Huang, H. Wu, H. Reeve, N.V. Vuong, and J.P. Liu, Thermal Stability of MnBi Magnetic Materials, *J. Phys.: Condens. Matter*, 2014, **26**, p 064212

6. Y.-C. Chen, G. Gregori, A. Leineweber, F. Qu, C.-C. Chen, T. Tietze, H. Kronmüller, G. Schütz, and E. Goering, Unique High-Temperature Performance of Highly Condensed MnBi Permanent Magnets, *Scr. Mater.*, 2015, **107**, p 131-135

7. M. Ellner, Über die kristallchemischen Parameter der Ni-, Co- und Fe- haltigen Phasen vom NiAs-Typ, *J. Less-Common Met.*, 1976, **48**, p 21-52 (in German)

8. R.G. Ross and W. Hume-Rothery, On the Equilibrium Diagram of the System Bismuth Rhodium, *J. Less-Common Met.*, 1962, **4**, p 454-459

9. V.G. Vanyarkho, N.A. Moshchalkova, V.M. Gunchenko, and N.V. Fadeeva, On the Existence of the Compound MnSb, *Izv. Akad. Nauk SSSR, Neorg. Mater.*, 1988, **24**(6), p 900-903, in Russian

10. K. Lee, J.C. Suits, and G.B. Street, Stabilization on the High Temperature Phase of MnBi by the Addition of Rhodium or Ruthenium, *Appl. Phys. Lett.*, 1975, **26**(2), p 27-29

11. V. Taufour, S. Thimmaiah, S. March, S. Saunders, K. Sun, T.N. Lamichhane, M.J. Kramer, S.L. Budko, and P.C. Canfield, Structural and Ferromagnetic Properties of an Orthorhombic Phase of MnBi Stabilized with Rh Addition, *Phys. Rev. Appl.*, 2015, **4**, p 014021

12. J.C. Suits, Ferromagnetism in Bi- and Te- Substituted MnRh, *IBM J. Res. Dev.*, 1975, **19**(4), p 422-423

13. G.B. Street, J.C. Suits, and K. Lee, New Compounds in the Mn-X-Bi System where X = Ni, Cu, Rh or Pd, *Solid State Chem.*, 1974, **14**(1), p 33-36

14. P. Kainzbauer, K.W. Richter, H.S. Effenberger, M.C.J. Marker, and H. Ipser, Single-Crystal Structure Determination of two New Ternary Bis–muthides: $Rh_6Mn_5Bi_{18}$ and $RhMnBi_3$, *Acta Cryst. C*, 2018, **74**(7), p 863-869

15. T.B. Massalski, H. Okamoto, P.R. Subramanian, and L. Kacprzak, Eds., Binary Alloy Phase Diagrams, 2nd ed., ASM International, Materials Park, OH, 1996, p 759-761; 2593-2595,

16. E. Raub and W. Mahler, Die Legierungen des Mangans mit Platin, Iridium, Rhodium und Rutenium, *Z. Metallk.*, 1955, **46**, p 282-290 (in German)

17. P. Kainzbauer, K.W. Richter, and H. Ipser, The Binary Bi-Rh Phase Diagram: Stable and Metastable Phases, *J. Phase Equilib. Diffus.*, 2018, **39**, p 17-34

18. B.W. Roberts, Neutron Diffraction Study of the Structures and Magnetic Properties of Manganese Bismuthide, *Phys. Rev.*, 1954, **104**(3), p 607-616

19. A.F. Andresen, W. Hälg, P. Fischer, and E. Stoll, The Magnetic and Crystallographic Properties of MnBi Studied by Neutron Diffraction, *Acta Chem. Scand.*, 1967, **21**(6), p 1543-1554

20. T. Chen, Contribution to Equilibrium Phase-Diagram of Mn-Bi System Near MnBi, *J. Appl. Phys.*, 1974, **45**, p 2358-2360

21. A.F. Andresen, J.E. Engebretsen, and J. Refsnes, Neutron Diffraction Investigations on Quenched MnBi and $MnBi_{0.9}Sb_{0.1}$, *Acta Chem. Scand.*, 1972, **26**, p 175-190

22. K. Cenzual, L.M. Gelato, M. Penzo, and E. Parthé, Inorganic Structure Types with Revised Space Groups. I, *Acta Cryst. B*, 1991, **47**, p 433-439

23. A. Hellawell, The Constitution of Manganese Base Alloys with Metals of the Second Transition Series, *J. Less Com. Met.*, 1959, **1**, p 343-347

24. A. Kussman, K. Müller, and H. Wollenberger, Property Changes in the Martensitic $\beta_1 \rightleftarrows \beta_2$ Transformation in the Rhodium-Manganese System, *Z. Angew. Phys.*, 1966, **20**(5), p 461-465

25. J.S. Kouvel, C.C. Hartelius, and L.M. Osika, Magnetic Properties and Crystal-Structure Transformation of the Ordered Alloy (MnRh), *J. Appl. Phys.*, 1963, **34**, p 1095-1096

26. Y. Nakayama and M. Asanuma, Magnetic Properties of Mn-Rh System Alloys, *Jpn. J. Appl. Phys.*, 1965, **4**, p 315-316

27. K. Selte, E. Bjerkelund, A. Kejekshus, A.F. Andresen, W.B. Pearson, and V. Meisalo, Equiatomic Transition Metal Alloys of Manganese VIII. Structural and Magnetic Proprties of Rh-Mn Phase, *Acta Chem. Scand.*, 1972, **26**, p 719-732

28. A. Sakuma, R.Y. Umetsu, and K. Fukamichi, Magnetic Structures and their Stability in Mn_3Rh Ordered and Disordered Alloys, *Phys. Rev. B*, 2002, **66**, p 014432

29. J. Wang, Z. Jiang, W. Chen, X. Zhang, and B. Zhou, The First-Principles Study of Martensitic Transformations in MnMe (Me = Rh, Pd) Alloys at Low Temperatures, *Intermetallics*, 2013, **34**, p 83-88

30. R. Yamauchi, K. Fukamichi, H. Yamauchi, K. Yamada, and K. Sasao, Large Spontaneous Volume Magnetostriction of Mn-Rh Alloys, *IEEE Trans. Magnet.*, 1999, **15**(5), p 3799-3801

31. R. Yamauchi, T. Hori, M. Miyakawa, and K. Fukamichi, Lattice Distortions and the Magnetic Susceptibility of γ-MnRh Disordered Alloys, *J. Alloys Compd.*, 2000, **309**, p 16-19

32. R. Yamauchi, K. Fukamichi, H. Yamauchi, A. Sakuma, and J. Echigoya, The Néel Temperature of $Mn_{100-x}Rh_x$ Alloys in Ordered and Disordered States, *J. Appl. Phys.*, 1999, **85**(8), p 4741-4743

33. R. Yamauchi, K. Fukamichi, H. Yamauchi, and A. Sakuma, Concentration Dependence of the Néel Temperature of $Mn_{100-x}Rh_x$ Ordered Alloys, *J. Alloys Compd.*, 1998, **279**, p 93-96

34. E. Krén, G. Kádár, L. Pál, J. Sólyom, and P. Szabó, Magnetic Structures and Magnetic Transformations in Ordered $Mn_3(Rh, Pt)$ Alloys, *Phys. Letters*, 1966, **20**(4), p 331-332

35. TOPAS 4.2, Bruker AXS Inc., Karlsruhe, Germany, 2011.

36. R.A. Robinson, A. Purwanto, M. Koghi, P.C. Canfield, T. Kamiyama, T. Ishigaki, J.W. Lynn, R. Erwin, E. Peterson, and R. Movshovich, Crystallography and Magnetism of the heavy-Fermion Compound Yb Bi Pt, *Phys. Rev. B*, 1994, **50**(13), p 9595-9598

37. T. Yamada, N. Kunitomi, Y. Nakai, D.E. Cox, and G. Shirane, Magnetic Structure of α-Mn, *J. Phys. Soc. Jpn.*, 1970, **28**(3), p 615-627

38. R.H. Schroeder, N. Schmitz-Pranghe, and R. Kohlhaas, Experimentelle Bestimmung der Gitterparameter der Platinmetalle im Temperaturbereich -190 bis 1709°C, *Z. Metallk.*, 1972, **63**, p 12-16 (in German)

39. M.J. Radler, J.B. Cohen, G.P. Sykora, T. Mason, D.E. Ellis, and J. Faber, Jr., The Defect Structures of $Mn_{1-x}O$, *J. Phys. Chem. Solid.*, 1992, **53**(1), p 141-154